

# Optical Nanomanipulations of Malignant Cells: Controlled Cell Damage and Fusion

Limor Minai, Daniella Yeheskely-Hayon, Lior Golan, Gili Bisker, Eldad J. Dann, and Dvir Yelin\*

*Specifically targeting and manipulating living cells is a key challenge in biomedicine and in cancer research in particular. Several studies have shown that nanoparticles irradiated by intense lasers are capable of conveying damage to nearby cells for various therapeutic and biological applications. In this work ultrashort laser pulses and gold nanospheres are used for the generation of localized, nanometric disruptions on the membranes of specifically targeted cells. The high structural stability of the nanospheres and the resonance pulse irradiation allow effective means for controlling the induced nanometric effects. The technique is demonstrated by inducing desired death mechanisms in epidermoid carcinoma and Burkitt lymphoma cells, and initiating efficient cell fusion between various cell types. Main advantages of the presented approach include low toxicity, high specificity, and high flexibility in the regulation of cell damage and cell fusion, which would allow it to play an important role in various future clinical and scientific applications.*

## 1. Introduction

The ability to noninvasively access and effectively manipulate cells with minimal damage to nearby tissue is one of the key challenges of modern approaches for cancer therapy. Conventional therapeutic procedures, often a combination of chemotherapy, radiotherapy, and surgery, are frequently invasive and nonspecific, causing collateral damage to normal viable tissues, which results in serious side effects in most patients. In an attempt to complement conventional treatments,

numerous new approaches for treating malignant cells with minimal collateral damage are constantly being studied and developed. Owing to its low toxicity to native tissue, laser light in the visible and near-infrared wavelength range is particularly attractive for manipulating tissue through specific intermediate agents. The strong local interaction between light and a photosensitizer, combined with a negligible interaction with healthy nearby tissue, make photodynamic therapy a favorable approach for treating several types of cancer with relatively few side effects.<sup>[1]</sup> Recently, several approaches for targeting cancer with low toxicity have been proposed, utilizing gold nanoparticles which are relatively inert and biocompatible, and can mediate the effect of light without the need of a toxic photosensitizer. Gold nanoparticles of various sizes and shapes, including spheres,<sup>[2]</sup> rods,<sup>[3,4]</sup> shells,<sup>[5,6]</sup> hollow shells,<sup>[7]</sup> cages,<sup>[8,9]</sup> and branched particles<sup>[10]</sup> have been proven useful in generating significant photothermal damage to cancer cells. Intense pulse lasers of pulses shorter than 10 ns<sup>[3,11–13]</sup> have been shown to induce different, more localized effects in tissues as compared to continuous-wave lasers,<sup>[14–17]</sup> either at the near-infrared wavelength range<sup>[4,18]</sup> or at the visible part of the spectrum.<sup>[2,15]</sup> Such effects, combined with specific localization of the mediating nanoparticles within the

Dr. L. Minai, Dr. D. Yeheskely-Hayon, L. Golan,  
G. Bisker, Dr. D. Yelin  
Department of Biomedical Engineering  
Technion-Israel Institute of Technology  
32000, Haifa, Israel  
E-mail: yelin@bm.technion.ac.il

Prof. E. J. Dann  
Department of Hematology and Bone Marrow Transplantation  
Blood Bank and Aphaeresis Unit; Rambam Medical Center and Bruce  
Rappaport Faculty of Medicine  
Technion, Haifa, Israel



DOI: 10.1002/sml.201102304

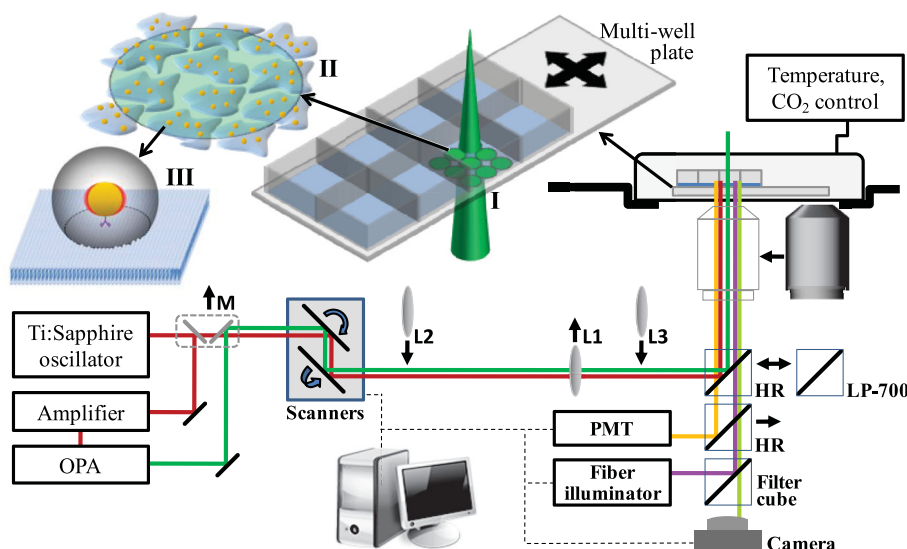


**Figure 1.** Schematic of the optical system for nanomanipulations of cells. A beam from an optical parametric amplifier (OPA) at wavelength 550 nm (green line) was scanning the sample using two scanning mirrors. A single lens (L1) was used to reduce the beam's diameter on the sample to 250–350  $\mu\text{m}$ . For two-photon imaging, the beam from the Ti:Sapphire oscillator was picked using a flipped mirror (M), scanned and magnified using lenses L2 and L3, and focused by inserting an objective lens before the sample. The two-photon fluorescence signal was detected by a photomultiplier tube (PMT) after replacing the high reflectivity (HR) mirror by a dichroic short-pass mirror (LP-700). After irradiation, time lapse imaging was conducted by replacing the dichroic mirror with different filter cubes optimized for the specific fluorescent markers that were used. Schematic illustrations show I) the irradiation pattern of the pulse beam, II) the irradiated nanoparticle-targeted cells, and III) the extent of the nanometric effect induced by each nanoparticle, including the near field enhancement beyond the ionization threshold (red regions), the spherical shock wavefront (gray sphere), and the affected area on the membrane (dashed circle).

cells, were recently shown capable of inducing different death mechanisms in cancer cells.<sup>[15,19]</sup>

These studies have attempted at maximizing the efficiency of the driving optical effect, while minimizing nonspecific effects by avoiding the use of toxic agents, employing specific biochemical targeting techniques, utilizing non-ionizing irradiation, and reducing potentially harmful photothermal effects. This approach for manipulating cells on a nanometric scale includes three main steps: conjugating gold nanoparticles to specific molecules with high affinity to the targeted cells, delivering these functionalized nanoparticles to the cells, and irradiating them by a series of intense pulses whose wavelength is tuned to the plasmonic resonance of the nanoparticles. The absorption of the laser pulses by a nanoparticle then leads to a rapid particle heating, resulting in an expanding wave front of hot vapor, accompanied by an acoustic pressure wave emitted by the sudden thermal expansion of the particle.<sup>[20]</sup> In addition, if pulse duration is sufficiently short, near-field enhancement on the particle's surface would exceed ionization threshold, forming low-density plasma within the expanding vapor around the particle. For pulse energies below certain values (typically on the order of a few  $\text{mJ}/\text{cm}^2$ ), the resulting bubbles would expand to only a few tens of nanometers in diameter, before collapsing and disappearing after 10–500 ns.<sup>[21]</sup>

In this work, we follow the same approach for cancer cell nanomanipulations, but choose to work with femtosecond pulses and gold nanospheres which are characterized by a much higher structural stability compared to other, non-spherical nanoparticles. Although femtosecond laser systems

at the visible range may be restrictive for some applications, we could obtain a high degree of control over the desired effect, allowing high repeatability even after several intense irradiation pulses. Our technique is demonstrated by selectively damaging or fusing cells of epidermoid carcinoma and B cell lymphoma, two types of malignancies of different origins and characteristic cell morphology. Our results reveal that the resulting outcome of the irradiation is highly sensitive to a range of irradiation parameters, allowing a high level of consistency and control over cell fate.

## 2. Results

Biochemical targeting of gold nanoparticles to epidermoid carcinoma (A431) and Burkitt lymphoma B (BJAB) cells was attained using particles which were coated with anti-EGFR antibody (EGFR is the epidermal growth factor receptor)<sup>[22,23]</sup> and chimeric anti-CD20 monoclonal antibody (Rituximab TM),<sup>[24]</sup> respectively. In order to irradiate the nanoparticle-targeted cells and continuously monitor the outcome, we have constructed a custom-built inverted microscope system (**Figure 1**) which, using a single platform, allows sample irradiation by single intense femtosecond pulses, two-photon excitation fluorescence microscopy, and time-lapse multichannel fluorescence imaging. Two-photon excitation fluorescence microscopy of nanoparticle-targeted A431 cells showed strong fluorescence signals emitted from the gold nanoparticles which were attached to the cell membranes (**Figure 2a**), while control cells without nanoparticles

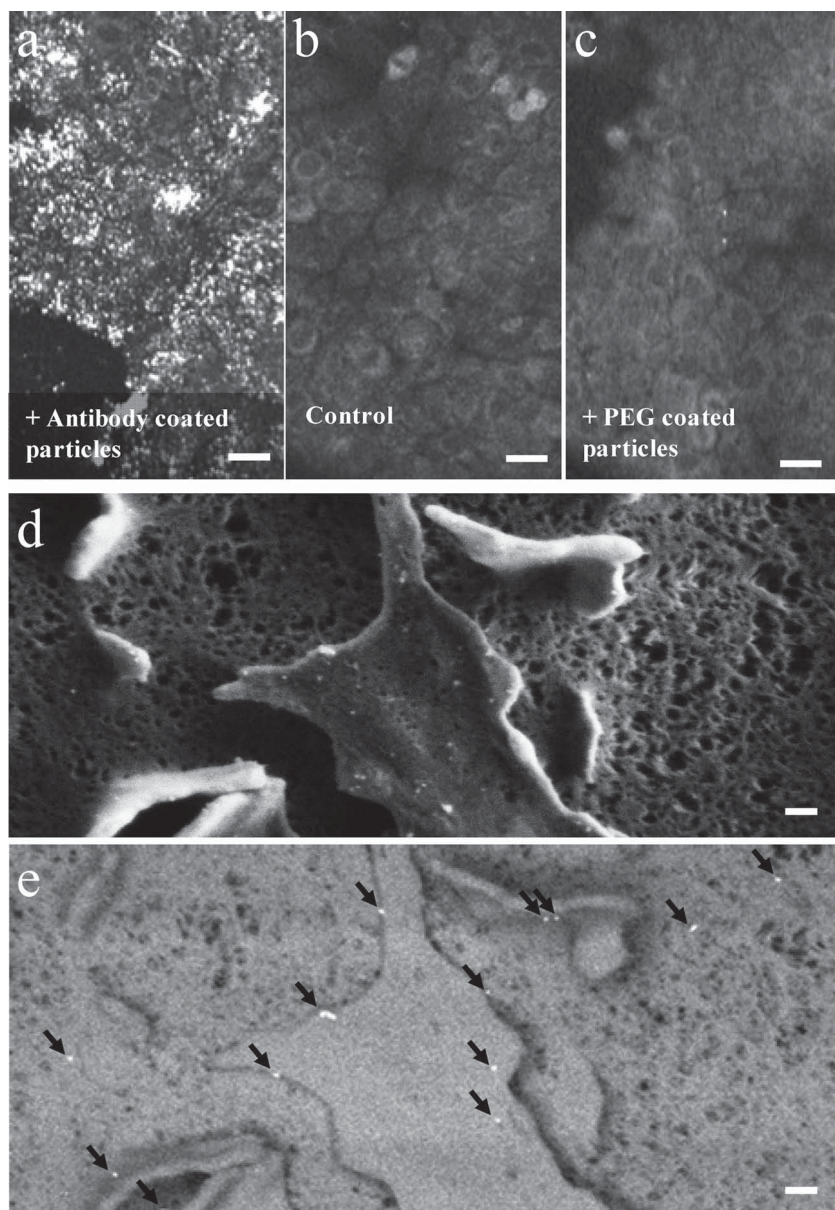


**Figure 2.** Gold nanoparticles on carcinoma cell membranes. Two-photon imaging of A431 cells incubated with a) anti-EGFR-coated gold nanoparticles, b) no nanoparticles, and c) PEG-coated gold nanoparticles. Scale bars in a–c represent 30  $\mu\text{m}$ . d) Scanning electron microscopy of a cell membrane targeted by anti-EGFR gold nanoparticles. e) Scanning electron microscopy using the back scattering detector reveals bright reflections indicative of gold particles (marked by arrows). Scale bars in d and e represent 100 nm.

(Figure 2b) or with nonspecific (polyethylene glycol (PEG)-coated) nanoparticles (Figure 2c) exhibited only a weak autofluorescence. Further confirmation of the specific binding of the nanoparticles-antibody conjugates to the cells was attained using scanning electron microscopy (SEM), which revealed small nanometric features on the cell membranes (Figure 2d) and identified their high atomic number (Figure 2e). The SEM images also revealed that nanoparticles were attached to the cells' membranes either as isolated individual particles, or in small aggregates (data not shown).

After being targeted by nanoparticles, cells were irradiated using a 50 fs pulse beam whose wavelength (550 nm)

was tuned to the plasmonic resonance of the nanoparticles. Widespread necrosis was evident in A431 cells which were incubated with anti-EGFR gold nanoparticles and irradiated by 16 pulses (35  $\text{mJ}/\text{cm}^2$  per pulse), 5 h after irradiation (Figure 3a and Supporting Information (SI), movie 1). Control cells which were not incubated with nanoparticles and irradiated with an identical pulse series showed only a small amount of necrotic and apoptotic cells (Figure 3b and SI, movie 2). Nanoparticle-targeted cells irradiated by 4 pulses showed insignificant necrosis rate 5 h after irradiation; instead, numerous neighboring cells have begun to fuse with each other, forming several giant multi-nucleated cells throughout the field of view (Figure 3c and SI, movie 3). Control cells with no nanoparticles which were irradiated by 4 pulses have shown no such behavior (Figure 3d and SI, movie 4). Using only a single pulse irradiation, no significant effect was observed in the nanoparticle-targeted cells after 5 h, however, the number of apoptotic cells increased significantly 23 h after irradiation (Figure 3e and SI, movie 5), in comparison to the control cells with no nanoparticles (Figure 3f and SI, movie 6). Large plasma membrane vesicles, or blebs, are clearly noticeable in Figure 3a, and to a lesser extent in Figure 3c and e, indicating the rupture of the cellular plasma membrane-cytoskeleton interface due to the combined effect of the pulse irradiation and the nanoparticles. Similar vesicles were previously observed in cells as a result of tightly focused femtosecond pulse beam irradiation.<sup>[13,25]</sup>

Quantitative analysis (Figure 4) of the cells undergoing necrosis, fusion, and apoptosis after irradiation by 16 pulses, 4 pulses, and 1 pulse reveals that cell fate could be controlled to a high degree by selecting a specific number of pulses for irradiation; nearly 90% of the cells became necrotic 5 h following irradiation by 16 pulses, 15%

of the cells were fused with nearby cells after 4 pulses, and 50% of the cells became apoptotic 23 h after a single pulse irradiation.

Experiments with Burkitt lymphoma cells have revealed similar results (Figure 5a) to those obtained with the epidermoid carcinoma cells. Incubation with Rituximab-coated nanoparticles did not appear to significantly affect BJAB cell viability following 20 min incubation (no irradiation), as compared to the control BJAB cells with no nanoparticles (Figure 5a, top panels). Indeed, in a heat-inactivated serum, the anti-CD20 antibody was not expected to induce immediate cellular damage to BJAB cells.<sup>[26]</sup> Nevertheless, aggregation of

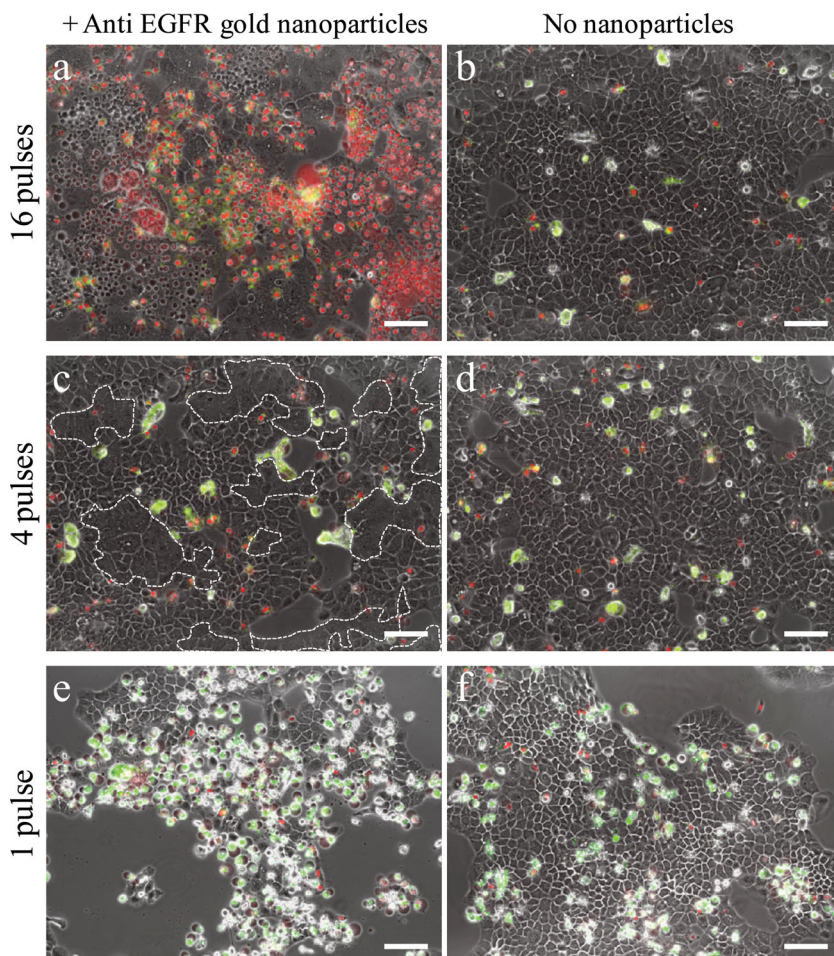


**Figure 3.** Damaging carcinoma cells using anti-EGFR-coated nanoparticles and resonance femtosecond pulse irradiation. a) Gold-nanoparticle-conjugated cells irradiated by 16 pulses. b) Nonconjugated cells, 16 pulses. c) Conjugated cells irradiated by 4 pulses. d) Nonconjugated cells, 4 pulses. e) Conjugated cells irradiated by 1 pulse. f) Nonconjugated cells, 1 pulse. Multi-nucleated cells margins are marked by dashed white curves in (c). Scale bars represent 50  $\mu\text{m}$ . Red nuclei indicate necrotic cells. Green stain indicates apoptosis. Panels a–d show cells 5 h after irradiation. Panels e,f show cells 23 h after irradiation.

the nanoparticle-targeted cells was evident (Figure 5a), a known occurrence often induced by Rituximab.<sup>[27]</sup> Irradiation of nanoparticle-targeted cells by 1 and 4 pulses has led to approximately 25% and 60% necrotic cells in the culture, respectively, nearly five times the measured rates at cells with no nanoparticles (Figure 5b). Increasing the number of irradiation pulses to 16 resulted in nearly 90% necrosis, independent of the presence of nanoparticles (Figure 5a, bottom panels). A bar-chart summarizing the necrosis rate for all samples (Figure 5b) demonstrates the important role of the gold nanoparticles in the induction of necrosis following 1- and 4-pulse irradiation. Further validation of these results was obtained using flow cytometry analysis of the entire irradiated suspensions (10 000 cells) 15 h post-irradiation (SI, Figure 1), which showed approximately 19%, 46% and 50%, necrosis following 1-, 4-, and 16-pulse irradiation, respectively.

To verify the specificity of the damage generated by anti-EGFR gold nanospheres to EGFR over-expressing cells, both A431 and BJAB cells were incubated with anti-EGFR gold nanoparticles, washed off the unbound particles, and

irradiated by 8 pulses for fusion induction (SI, Figure S2) or by 10 pulses for necrosis induction (SI, Figure S3). While 20% of the A431 cells, which are known to over-express EGFR on their plasma membrane, have been fused together 3 h after irradiation (SI, Figure S2b), BJAB cells incubated with anti-EGFR nanoparticles did not show any noticeable effect (SI, Figure S2d). Similarly, A431 cells incubated with anti-EGFR gold nanoparticles and irradiated by 10 pulses showed 50% necrosis 30 min after irradiation (SI, Figure S3b), while irradiated BJAB cells which were incubated with the same particles did not show noticeable effect (SI, Figure S3d).

In order to demonstrate specificity between cells of similar type, BJAB cells and K562 myelogenous leukemia cells, which do not express CD20, were both incubated with anti-CD20 gold nanoparticles and irradiated by 5 pulses after washing off the unbound particles. Phase and fluorescence microscopy images of the cell lines have shown significant necrosis of BJAB cells (SI, Figure S4b) and no apparent necrosis of the K562 cells which do not express CD20 (SI, Figure S4e). Flow cytometry analysis of the cells' viability has confirmed the difference in necrosis rates, showing 38% BJAB cell necrosis 17 h following irradiation (SI, Figure S4c) and only 3.2% necrosis in the K562 cells (SI, Figure S4f).

In addition to the number of irradiating pulses, the amount of energy delivered by each individual pulse provides yet another means for optimizing a desired

outcome. In order to study the effect of pulse energy, fusion and necrosis rates of irradiated BJAB cells were quantified

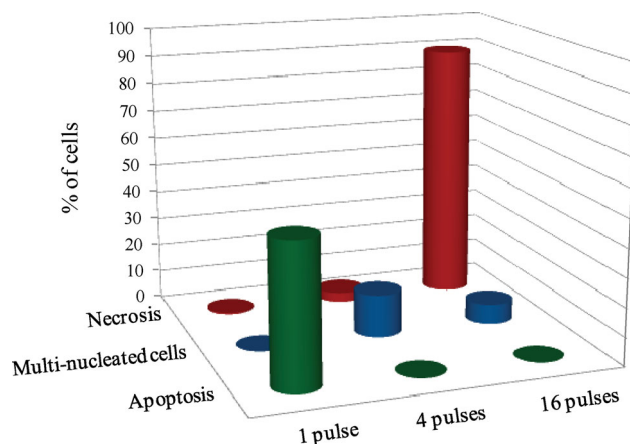


**Figure 4.** Percentage of cells undergoing necrosis (red bars), fusion (blue bars), and apoptosis (green bars) as a function of the number of irradiating pulses.

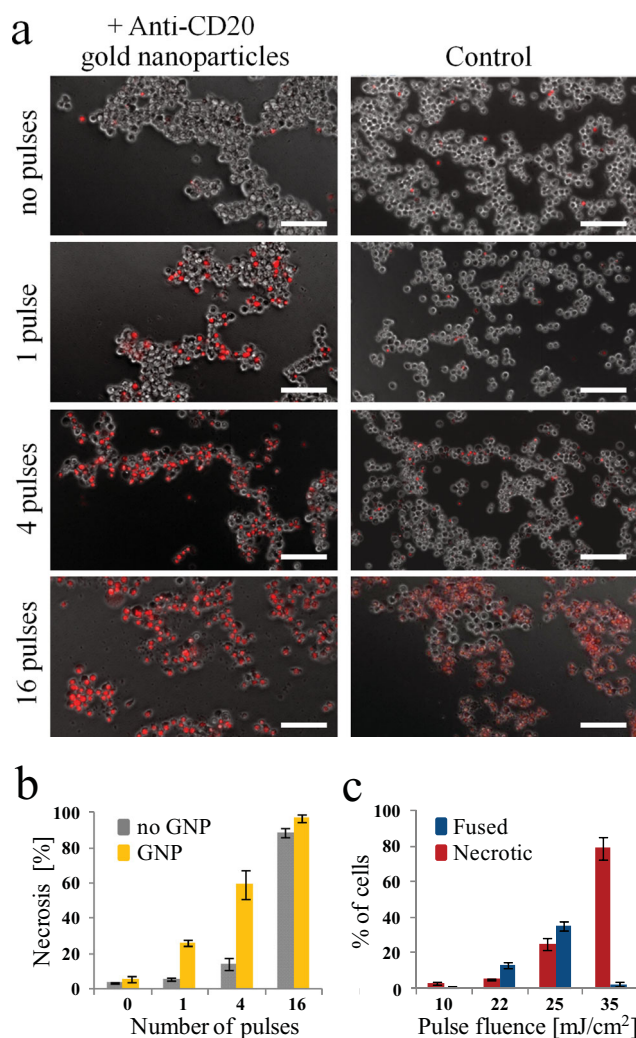


**Figure 5.** Effect of resonance pulse irradiation on necrosis and fusion of specifically targeted lymphoma B cells. a) Fluorescence images of propidium iodide (indicating necrotic cells) distribution superimposed on phase contrast images, 15 h following irradiation by sequences of 1, 4, and 16 pulses. Scale bars represent 70  $\mu\text{m}$ . b) Bar chart summarizing the percentage of necrotic cells in (a). c) Bar chart summarizing the percentage of necrotic and fused lymphoma B cells irradiated by 16 pulses, as a function of increasing pulse fluence. The numbers of necrotic cells and fused cells were evaluated 15 h and 1 h post-irradiation, respectively. GNP refers to gold nanoparticles.

for different pulse fluence levels, while the number of irradiating pulses was kept constant (16 pulses) for all experiments. Below 10  $\text{mJ}/\text{cm}^2$  per pulse in a series of 16 pulses, no multi-nucleated cells were observed and a negligible increase (less than 3%) in necrosis rate was evident (Figure 5c). At 25  $\text{mJ}/\text{cm}^2$  per pulse, the fusion rate reached a peak value of 35% of the cells, 30% higher than the fusion rate obtained at 35  $\text{mJ}/\text{cm}^2$  per pulse. Pulse fluence above 35  $\text{mJ}/\text{cm}^2$  caused widespread cell death (mainly necrosis) throughout the sample, similar to the results obtained with the epidermoid carcinoma cells (Figure 3a).

For applications which do not require high degree of specificity, we have found that cell fusion and necrosis could be induced merely by adding nonspecific (no targeting molecule) gold nanoparticles to the cells' growth medium, and

irradiating the cells without washing the unbound gold, using pulse parameters (wavelength, fluence, pulse number) that are similar to those used with antibody-conjugated particles. A closer look (Figure 6a) at the process of a fusion event mediated by nonspecific particles, after 5 pulse irradiation of 35  $\text{mJ}/\text{cm}^2$  per pulse, reveals the gradual formation of a multi-nucleated cell from four identical BJAB cells whose nuclei were labeled with different blue and red fluorescent dyes. The fusion process, as captured in a sequence of fluorescence images superimposed on phase contrast images (Figure 6a), was nearly completed three minutes after irradiation, as evident by the apparent uniform plasma membrane (green) surrounding the four nuclei. Cell proximity was found to play a crucial role in the fusion process; multinucleated cells comprising of up to 20 nuclei were observed in several experiments, depending mainly on the mutual proximity of the individual cells prior to irradiation.

One potentially important application for controlled induction of cell fusion is the generation of a hybrid cell (often termed 'hybridoma') from an antibody-producing B cell and a myeloma cell. At present, techniques for producing hybridoma cells, which are a key tool for the production of monoclonal antibodies,<sup>[28]</sup> commonly involve the use of PEG,<sup>[29]</sup> electrofusion<sup>[30]</sup> and the use of viruses.<sup>[31]</sup> In order to demonstrate the potential of our approach to form hybridoma cells, a mixture of B cells of human origin (BJAB cells, red stained nuclei) and myeloma cells of murine origin (NSO cells, blue stained nuclei) were incubated in a medium containing non-specific nanoparticles and irradiated by 5 pulses (35  $\text{mJ}/\text{cm}^2$  per pulse) at resonance (550 nm) wavelength. A time sequence image (Figure 6b) demonstrating fusion between a B cell and a myeloma cell shows that nuclei of both cells were completely engulfed by a uniform, single membrane, less than eight minutes past irradiation. In this experiment, fusion rate was low (3–6%) compared to the fusion rate between two B cells of human origin, but consistent with similar experiments performed with a homogeneous murine cell culture (data not shown). The majority of the fused cells have survived 24 h after the fusion, based on visual examination of their morphology. A further study of these hybridomas would need to be conducted in order to test their viability and their ability to effectively produce antibodies. Several techniques could be applied in order to increase fusion rates, including the use of repetitive irradiation sequences, and adjustment of the various biological and physical parameters of the experiments.

### 3. Discussion

Adjusting the optical parameters of the irradiating femto-second pulses provide valuable control over the process of nanomanipulations of malignant cells, which could be utilized for effective cancer therapy either by removing cancerous tissue by inducing different cell death mechanisms, or by effectively fusing cells of the immune system with tumor cells to produce anti-cancer vaccination.<sup>[32,33]</sup> The high level of control and repeatability obtained in this work was mainly due to the high structural and optical stability of the gold nanospheres, which have maintained their shape after each

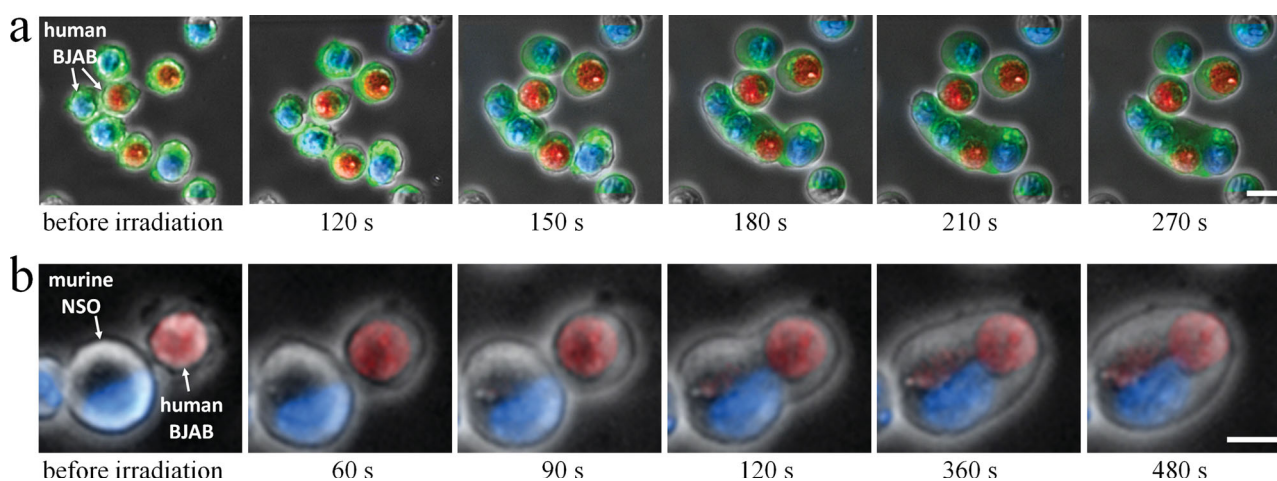


**Figure 6.** Induction of cell fusion. a) Time sequence of fluorescence images of fusing B (BJAB) cells superimposed on phase contrast images, following irradiation by 5 pulses in the presence of nonspecific gold nanoparticles. Plasma membranes were labeled green. Nuclei were labeled either blue or red. b) Formation of a hybridoma cell. Time sequence of fluorescence images of human B (BJAB) cells (red nuclei) and murine myeloma (NSO) cells (blue nuclei) superimposed on phase contrast images, following irradiation by 5 pulses in the presence of nonspecific gold nanoparticles. Scale bars represent 10  $\mu\text{m}$ .

individual pulse, even though their temperature has crossed the melting point. Working with gold nanospheres, however, limits the choice of wavelength to the visible range, which is less favorable for deep tissue penetration. We have been experimenting with cell-lines which represent two different types of malignancies that could be easily accessed by visible light; one of epithelial origin, the other of lymphoid origin. Our approach would therefore be limited to superficial tissue or to *ex vivo* applications where cells are extracted from the patient.

The exact interaction between nanometric shockwaves and cells depends on numerous physical and biological parameters. While we have shown that the number of pulses and their fluence could considerably affect cell fate, many other parameters of this technique are still left unexplored, including pulse repetition rate, pulse duration and wavelength, as well as the particles' size, shape, concentration, coating layer, and distribution within the cells. In a recent theoretical work<sup>[20]</sup> it has been hypothesized that nanosurgery can be conducted using femtosecond pulses with fairly low pulse energies; however, the role of multiphoton ionization produced by the surface-enhanced optical fields has not been considered. Further theoretical and experimental studies are required in order to determine whether and how low density plasma generated around a particle would affect cellular organelles.

The exact desired effects to be induced on the cells depend on various factors which stem from the chosen treatment plan. Chemotherapy and radiation therapy are often used to induce apoptosis in rapidly dividing cells<sup>[34,35]</sup> in order to promote tumor death. However, the inherent anti-apoptotic mechanisms of numerous types of malignant cells often require overly aggressive treatments, limiting the effectiveness of these approaches. Specific induction of apoptosis would be beneficial for clinical applications that are sensitive to inflammation which could occur due to uncontrolled spillage of cellular content.<sup>[36]</sup>

For malignant tumors which exhibit high level of resistance to apoptosis,<sup>[35]</sup> the induction of necrosis rather than apoptosis, is often preferred. Moreover, previous studies have shown that necrotic cellular death is effective for the activation of the immune system.<sup>[37–39]</sup> An important example for such an application is the use of necrotic tumor cell lysates for the production of cancer vaccines, which are used to stimulate the immune system of chronic B lymphocytic leukemia patients to detect and attack 'self' cancerous B cells.<sup>[40,41]</sup> The potential use of Rituximab, an FDA approved anti-CD20 monoclonal antibody drug for the treatment of B-cell leukemia and non-Hodgkin lymphomas, for targeting gold nanoparticles to B cells is particularly advantageous for such an application, as the antibody molecules would further enhance and complement the effect of the laser pulses.

Specific induction of cell fusion could be useful for numerous applications in drug development and cancer research. Conventional methods for cell fusion often involve the addition of PEG to the cell medium,<sup>[42]</sup> application of a high voltage across the cells' plasma membranes,<sup>[30]</sup> and the use of viruses.<sup>[31]</sup> A tightly focused femtosecond laser beam<sup>[43]</sup> has also been shown capable of fusing neighboring cells by rupturing their membranes at specific locations.<sup>[44,45]</sup> These techniques, however, are inadequate for fusing a specific type of cells within diverse cell populations. Specific fusion could be important, for example, for generating hybridoma cells for the production of monoclonal antibodies, and for the generation of autologous cancer vaccination by fusing cancer cells with dendritic cells.<sup>[32,33,46]</sup> Using nanoparticles with specific targeting antibodies allows our technique to affect only selected cells, and avoid significant collateral damage to nearby cells and tissue. The exact mechanism that governs the observed cell fusion is yet unclear, and while parallel nanometric ruptures of the plasma membrane is a likely explanation,<sup>[47]</sup> other biological and chemical factors may play a role in the process. In summary, we have presented a novel technology for manipulating cells in a nanometric scale

using antibody-conjugated gold nanospheres irradiated by single, intense, resonant femtosecond pulses. By controlling the flow rate of the optical energy to the targeted cells, we demonstrate a unique ability to specifically induce death or fuse cells from a selected cell population. The technique has been shown promising for numerous cancer-related therapeutic applications and would open new possibilities in biotechnology and in fundamental biological research.

## 4. Experimental Section

**Cell Cultures:** A431 epidermoid carcinoma cells (ATCC) were grown in Dulbecco's modified eagle medium (DMEM, Invitrogen) supplemented with 10% heat-inactivated fetal bovine serum, and 1 mM sodium pyruvate. BJAB and NSO cells were grown in RPMI-1640 medium (Sigma) supplemented with 2 mM glutamine and 5 mM sodium pyruvate. 10% heat-inactivated fetal bovine serum was added to BJAB cell culture and 10% heat-inactivated horse serum was added to NSO cell culture. BJAB and NSO cells were maintained at a concentration below  $10^6$  cells/mL to allow logarithmic growth. All cells were grown at 37 °C and 5% CO<sub>2</sub>.

**Nanoparticle Preparation:** Gold nanoparticles were prepared using the citrate reduction protocol<sup>[48,49]</sup> resulting in an average particle diameter of 20 nm. PEG coating was obtained by overnight incubation of the nanoparticles with  $7.5 \times 10^{-3}$  mM PEG-TA (where TA is thiotic acid; molecular weight, MW 2000; Jenkem) followed by three phosphate buffered saline (PBS) washes of unbound PEG. Addition of  $6.6 \times 10^{10}$  PEG-coated nanoparticles per ml to the growth medium of both carcinoma and lymphoma cells did not cause any visible effect (fusion, cell death) to the cells. Anti-CD20 (Rituximab, Roche Israel) coating of gold nanoparticles was carried out according to Weiss et al.<sup>[50]</sup> Anti-EGFR (Lab Vision, clone designation EGFR.1)-coated gold nanoparticles (20 nm average diameter) were custom made by Millennium Biotechnology Inc.

**Cell Targeting by the Nanoparticles:** A431 cells (80–90% confluency) were incubated for 1 h at 37 °C with  $1.5 \times 10^{11}$  anti-EGFR-coated gold nanoparticles per milliliter. BJAB cells ( $10^6$  cells per mL) were incubated for 20 min at 37 °C with  $4.5 \times 10^9$  Rituximab-coated gold nanoparticles per milliliter. Cells were washed off unbound gold nanoparticles (three PBS washes) prior to laser irradiation. Specific binding of the Rituximab-coated nanoparticles to the BJAB cells was verified using dark-field microscopy. For experiments with nonspecific cell targeting, PEG-coated gold nanoparticles were used at a concentration of  $6.6 \times 10^{10}$  mL<sup>-1</sup>.

**Fluorescence Labeling:** Cells were stained for apoptosis and necrosis using Annexin V and propidium iodide kit (Roche). For the fusion experiments, nuclei were stained with either DAPI at 2 µg/mL concentration (Sigma), Hoechst 33342 at 2 µg/mL (Sigma), or 10 mM Doxorubicin (Sigma). Cell membranes were stained using  $2 \times 10^{-6}$  M PKH67 (Sigma).

**Laser Pulse Irradiation:** A beam from a Ti:sapphire oscillator (Tsunami, Spectra Physics) was amplified (Spitfire Pro XP, Spectra Physics) and wavelength-tuned to 550 nm using an optical parametric amplifier (Topas-C, Spectra Physics). Pulse duration was 50 fs, at 1 kHz repetition rate. Cells were irradiated within 8-well chamber slides (Lab-Tek II, Thermo-scientific) which were placed within a microscope incubator (Okolab Inc.) at controlled temperature and CO<sub>2</sub> concentration. Irradiation pattern was either

a  $10 \times 10$  rectangular array of 350 µm diameter spots (approximately 12 mm<sup>2</sup> total area) or a  $35 \times 35$  rectangular array of 250 µm diameter spots (approximately 75 mm<sup>2</sup> total area) for the A431 and BJAB cell cultures respectively. Multiple pulse irradiations per spot were achieved by scanning the beam at lower rates, so that each point was irradiated by several consequent overlapping spots.

**Two-Photon Microscopy:** The beam from a Ti:sapphire oscillator (25 fs, 80 MHz, 800 nm) was scanned using two galvanometric scanners (Cambridge Technology), magnified and focused onto the sample using a 60×, numerical aperture, NA = 1.4 objective. Average power on the sample was approximately 16.5 mW. The two-photon excited fluorescence was filtered using a short-pass dichroic mirror (dcspxr700, Chroma technology) and a barrier filter (E680SP-2P, Chroma technology), and measured using a photomultiplier tube (H7422-40, Hamamatsu photonics). Each image represents a z-projection of a data cube which contains twenty  $500 \times 500$  pixel frames, each captured at 0.5 µm intervals along the z axis. Acquisition time was 50 s per frame.

**Time-Lapse Imaging:** Time-lapse imaging was controlled using NIS-Elements Advanced Research (Nikon) software. Frame rate was 3 min<sup>-1</sup> during the first 10 h of each experiment, followed by a frame rate of 1 h<sup>-1</sup> during the rest of the imaging period.

**SEM:** A431 cells were fixated using 3% glutaraldehyde and 1% osmium<sup>[51,52]</sup> on silicon chips (Ted Pella, Inc.). The microscope system used (Zeiss Ultra Plus HRSEM) was equipped with a Schottky field-emission electron gun and BalTec VCT100 cold-stage maintained at (–150 °C).

**Data Analysis:** Selected images of A431 cells acquired 5 h and 23 h after irradiation were used to quantitatively assess necrosis and apoptosis ratios using NIS-Elements Advanced Research (Nikon) software. The ratio of damaged cells within each frame was measured for each set of irradiation parameters and normalized according to the corresponding control experiments. Cell fusion was evaluated by manual counting and segmentation of the fused cells. Selected images of BJAB cells 15 h after irradiation were used to evaluate necrosis percentage. Cell fusion rate was measured by manual counting of the fusing cells using the entire time-lapse data sets. Quantification of necrosis in large populations of BJAB cells was conducted using fluorescence-activated cell sorting (BD FACS Calibur), in which cells were first stained using 1 µg/mL propidium iodide and then detected using 488 nm excitation wavelength. Results were analyzed using cyflogic software (CyFlo Ltd).

## Supporting Information

Supporting Information is available from the Wiley Online Library or from the author.

## Acknowledgements

The authors thank Prof. Gera Eytan for stimulating discussions. The research was funded by the European Research Council starting grant (number 239986).

- [1] P. Agostinis, K. Berg, K. A. Cengel, T. H. Foster, A. W. Girotti, S. O. Gollnick, S. M. Hahn, M. R. Hamblin, A. Juzeniene, D. Kessel, M. Korbelik, J. Moan, P. Mroz, D. Nowis, J. Piette, B. C. Wilson, J. Golab, *CA Cancer J. Clin.* **2011**, *61*, 250.
- [2] I. H. El-Sayed, X. Huang, M. A. El-Sayed, *Cancer Lett.* **2006**, *239*, 129.
- [3] J. L. Li, D. Day, M. Gu, *Adv. Mater.* **2008**, *20*, 3866.
- [4] X. Huang, I. H. El-Sayed, W. Qian, M. A. El-Sayed, *J. Am. Chem. Soc.* **2006**, *128*, 2115.
- [5] D. P. O'Neal, L. R. Hirsch, N. J. Halas, J. D. Payne, J. L. West, *Cancer Lett.* **2004**, *209*, 171.
- [6] S. Lal, S. E. Clare, N. J. Halas, *Acc. Chem. Res.* **2008**, *41*, 1842.
- [7] G. B. Braun, A. Pallaoro, G. Wu, D. Missirlis, J. A. Zasadzinski, M. Tirrell, N. O. Reich, *ACS Nano* **2009**, *3*, 2007.
- [8] J. Chen, D. Wang, J. Xi, L. Au, A. Siekkinen, A. Warsen, Z.-Y. Li, H. Zhang, Y. Xia, X. Li, *Nano Lett.* **2007**, *7*, 1318.
- [9] L. Au, D. Zheng, F. Zhou, Z.-Y. Li, X. Li, Y. Xia, *ACS Nano* **2008**, *2*, 1645.
- [10] B. Van de Broek, N. Devoogdt, A. D'Hollander, H.-L. Gijst, K. Janst, L. Lagae, S. Muyldermans, G. Maes, G. Borghs, *ACS Nano* **2011**, *5*, 4319.
- [11] H. Takahashi, T. Niidome, A. Nariai, Y. Niidome, S. Yamada, *Chem. Lett.* **2006**, *35*, 500.
- [12] X. Huang, W. Qian, I. H. El-Sayed, M. A. El-Sayed, *Lasers Surgery Med.* **2007**, *39*, 747.
- [13] L. Tong, Y. Zhao, T. B. Huff, M. N. Hansen, A. Wei, J. X. Cheng, *Adv. Mater.* **2007**, *19*, 3136.
- [14] G. S. Terentyuk, G. N. Maslyakova, L. V. Suleymanova, N. G. Khlebtsov, B. N. Khlebtsov, G. G. Akchurin, I. L. Maksimova, V. V. Tuchin, *J. Biom. Optics* **2009**, *14*, 021016-1.
- [15] X. Huang, B. Kang, W. Qian, M. A. Mackey, P. C. Chen, A. K. Oyelere, I. H. El-Sayed, M. A. El-Sayed, *J. Biomed. Optics* **2010**, *15*, 058002-1.
- [16] V. Raji, J. Kumar, C. S. Rejija, M. Vibin, V. N. Sheno, A. Abraham, *Exp. Cell Res.* **2011**, *317*, 2052.
- [17] W. I. Choi, J.-Y. Kim, C. Kang, C. C. Byeon, Y. H. Kim, G. Tae, *ACS Nano* **2011**, *5*, 1995.
- [18] P. Diagaradjane, A. Shetty, J. C. Wang, A. M. Elliott, J. Schwartz, S. Shentu, H. C. Park, A. Deorukhkar, R. J. Stafford, S. H. Cho, J. W. Tunnell, J. D. Hazle, S. Krishnan, *Nano Lett.* **2008**, *8*, 1492.
- [19] M. Gu, H. C. Bao, J. L. Li, *J. Biomed. Optics* **2010**, *15*, 050502-1.
- [20] A. N. Volkov, C. Sevilla, L. V. Zhigilei, *Appl. Surf. Sci.* **2007**, *253*, 6394.
- [21] E. Lukianova-Hleb, Y. Hu, L. Latterini, L. Tarpani, S. Lee, R. A. Drezek, J. H. Hafner, D. O. Lapotko, *ACS Nano* **2010**, *4*, 2109.
- [22] M. M. Wrann, C. F. Fox, *J. Biol. Chem.* **1979**, *254*, 8083.
- [23] A. Ullrich, L. Coussens, J. S. Hayflick, T. J. Dul, A. Gray, A. W. Tam, J. Lee, Y. Yarde, T. A. Libermann, J. Schlessinger, J. Downward, E. L. V. Mayes, N. Whittle, M. D. Waterfield, P. H. Seeburg, *Nature* **1984**, *309*, 418.
- [24] A. J. Grillo-López, C. A. White, C. Varns, D. Shen, A. Wei, A. McClure, B. K. Dallaire, *Semin. Oncol.* **1999**, *26*, 66.
- [25] C. Kelly, M.-M. Kober, P. Kinnunen, D. Reis, B. Orr, M. Banaszak Holl, *J. Biol. Phys.* **2009**, *35*, 279.
- [26] M. D. Pescovitz, *Am. J. Transplant.* **2006**, *6*, 859.
- [27] E. Cittera, C. Onofri, M. D'Apolito, G. Cartron, G. Cazzaniga, L. Zelante, P. Paolucci, A. Biondi, M. Introna, J. Golay, *Cancer Immunol. Immunotherapy* **2005**, *54*, 273.
- [28] G. Kohler, C. Milstein, *Nature* **1975**, *256*, 495.
- [29] B. R. Lentz, *Eur. Biophys. J.* **2007**, *36*, 315.
- [30] U. Zimmermann, *Biochim. Biophys. Acta - Rev. Biomembr.* **1982**, *694*, 227.
- [31] S. Nagata, K. Yamamoto, Y. Ueno, T. Kurata, J. Chiba, *Hybridoma* **1991**, *10*, 369.
- [32] B. Vasir, V. Borges, Z. Wu, D. Grosman, J. Rosenblatt, M. Irie, K. Anderson, D. Kufe, D. Avigan, *Br. J. Haematol.* **2005**, *129*, 687.
- [33] J. Rosenblatt, B. Vasir, L. Uhl, S. Blotta, C. MacNamara, P. Somaiya, Z. Wu, R. Joyce, J. D. Levine, D. Dombagoda, Y. E. Yuan, K. Francoeur, D. Fitzgerald, P. Richardson, E. Weller, K. Anderson, D. Kufe, N. Munshi, D. Avigan, *Blood* **2011**, *117*, 393.
- [34] J. F. R. Kerr, C. M. Winterford, B. V. Harmon, *Cancer* **1994**, *73*, 2013.
- [35] R. W. Johnstone, A. A. Ruefli, S. W. Lowe, *Cell* **2002**, *108*, 153.
- [36] D. A. Nelson, E. White, *Genes Dev.* **2004**, *18*, 1223.
- [37] S. Gallucci, M. Lolkema, P. Matzinger, *Nat. Med.* **1999**, *5*, 1249.
- [38] B. Sauter, M. L. Albert, R. Francisco, M. Larsson, S. Somersan, N. Bhardwaj, *J. Exp. Med.* **2000**, *191*, 423.
- [39] P. Mroz, J. T. Hashmi, Y. Y. Huang, N. Lange, M. R. Hamblin, *Expert. Rev. Clin. Immunol.* **2011**, *7*, 75.
- [40] K. Suresh, G. Fraser, E. Scheid, B. Leber, J. Gaudie, R. Foley, *Leukemia Lymphoma* **2006**, *47*, 297.
- [41] I. Hus, M. Schmitt, J. Tabarkiewicz, S. Radej, K. Wojas, A. Bojarska-Junak, A. Schmitt, K. Giannopoulos, A. Dmoszynska, J. Rolinski, *Leukemia* **2008**, *22*, 1007.
- [42] W. Gerhard, C. M. Croce, D. Lopes, H. Koprowski, *Proc. Nat. Acad. Sci. USA* **1978**, *75*, 1510.
- [43] A. Vogel, J. Noack, G. Hüttman, G. Paltauf, *Appl. Phys. B: Lasers Opt.* **2005**, *81*, 1015.
- [44] R. W. Steubing, S. Cheng, W. H. Wright, Y. Numajiri, M. W. Berns, *Cytometry* **1991**, *12*, 505.
- [45] K. Kuetemeyer, A. Lucas-Hahn, B. Petersen, H. Niemann, A. Heisterkamp, *J. Biomed. Opt.* **2011**, *16*, 088001-1.
- [46] E. Wieckowski, G. S. Chatta, R. M. Mailliard, W. Gooding, K. Palucka, J. Banchemareau, P. Kalinski, *Prostate* **2011**, *71*, 125.
- [47] G. Wu, A. Mikhailovsky, H. A. Khant, C. Fu, W. Chiu, J. A. Zasadzinski, *J. Am. Chem. Soc.* **2008**, *130*, 8175.
- [48] J. Turkevich, P. C. Stevenson, J. Hillier, *J. Phys. Chem.* **1953**, *57*, 670.
- [49] F. Porta, G. Speranza, Z. Krpetic, V. Dal Santo, P. Francescato, G. Scari, *Mater. Sci. Eng. B* **2007**, *140*, 187.
- [50] A. Weiss, T. C. Preston, J. Popov, Q. Li, S. Wu, K. C. Chou, H. M. Burt, M. B. Bally, R. Signorell, *J. Phys. Chem. C* **2009**, *113*, 20252.
- [51] L. Shaulov, R. Gruber, I. Cohen, A. Harel, *J. Cell. Sci.* **2011**, *124*, 3822.
- [52] U. Heinzmann, H. Höfler, *Histochem. Cell Biol.* **1994**, *101*, 127.

Received: October 31, 2011  
 Revised: December 21, 2011  
 Published online: